

Revealing the Effect of Nanoscopic Design on the Charge Carrier Separation Processes in Semiconductor-Metal Nanoparticle Gel Networks

Jakob Schlenkrich, Dániel Zámbo, Anja Schlosser, Pascal Rusch, and Nadja C. Bigall*

In this paper, it is shown that the nanoscopic design of combining semiconductors and noble metals has a direct impact on the macroscopic (electrochemical) properties of their assembled, hyperbranched, macroscopic gel networks. Controlled and arbitrary deposition of gold domains on CdSe/CdS nanorods leads to tipped and randomly decorated heteroparticles, respectively. Structural and optical properties of the gel networks depend upon assembling the hybrid particles by means of oxidative or ionic routes. Additionally, the impact of different building block designs on the charge carrier separation processes is investigated from spectroelectrochemical point of view. A more efficient charge carrier separation is revealed in the tipped design manifesting in higher negative photocurrent efficiencies compared to the arbitrary decoration, where the charge recombination processes are more remarkable. This work sheds light on the importance of the nanostructuring on the spectroelectrochemical properties at the macroscale paving the way towards their use in photochemical reactions.

approach towards novel hybrid functional materials with unique properties, which differ from those of colloidal mixtures of the two materials.^[1–3] The synthesis of these hybrid nanomaterials is often challenging due to different lattice dimensions, thermal stability, or chemical reactivity.^[4] Nevertheless, various combinations of different materials have already been synthesized and their promising properties have been demonstrated.^[4,5] Combining a semiconductor and a (noble) metal at the nanoscale results in hybrid nanostructures with advantageous properties for potential applications in photocatalysis, photoelectrochemical sensing, and photovoltaic applications.^[6–10] To date, the importance of the design at the nanoscale (i.e., engineering the components towards different hybrid-particles) has mainly been demonstrated at the single particle

1. Introduction


Combining different material classes at the nanoscale (such as metals with magnetic materials, semiconductors with magnetic materials or semiconductors with metals) is a promising

level and in solution-based ensembles.^[11–13] In semiconductor-metal hybrid nanoparticles, the photoelectrochemical performance relies on the efficient charge carrier separation and the utilization of the photogenerated electrons and holes in further reactions which is the major requirement for the above-mentioned applications.^[14] CdSe/CdS nanorods (NRs) alone offer some extent of charge carrier separation due to a negligible energy difference between the conduction band of CdSe and CdS and the resulting delocalization of the photoexcited electrons through the heterojunction and thus over the entire NR. Due to this special band alignment, this material combination behaves as a quasi-type II heterojunction.^[15] However, growing, e.g., gold on the semiconductor NRs leads to hybrid nanoparticles exhibiting further enhanced separation of the excited electrons and the holes within the different materials which enables the usage of these charge carriers in redox reactions.^[16] Nanostructural properties have remarkable impact on the overall optical or electrochemical response of the built-up macrostructures. We have shown recently that the number of gold nanoparticles relative to CdSe/CdS nanorods essentially governs the optical properties of macroscopic gel structures prepared by the cogelation of the two components.^[17] However, prior to the assembly, design of hybrid building blocks at the nanoscale (that is in terms of spatial distribution of the noble metal domains) is of great importance as well. These hybrid nanomaterials as ligand stabilized NPs in solution are usually restricted to solution-based applications, or the active

J. Schlenkrich, D. Zámbo, A. Schlosser, P. Rusch, N. C. Bigall
Institute of Physical Chemistry and Electrochemistry
Leibniz Universität Hannover
Callinstr. 3A, 30167 Hannover, Germany
E-mail: nadja.bigall@pci.uni-hannover.de

A. Schlosser, P. Rusch, N. C. Bigall
Laboratory for Nano and Quantum Engineering
Leibniz Universität Hannover
Schneiderberg 39, 30167 Hannover, Germany
N. C. Bigall

Cluster of Excellence PhoenixD (Photonics, Optics and Engineering –
Innovation Across Disciplines)
Leibniz Universität Hannover
30167 Hannover, Germany

 The ORCID identification number(s) for the author(s) of this article can be found under <https://doi.org/10.1002/adom.202101712>.

© 2021 The Authors. Advanced Optical Materials published by Wiley-VCH GmbH. This is an open access article under the terms of the Creative Commons Attribution-NonCommercial License, which permits use, distribution and reproduction in any medium, provided the original work is properly cited and is not used for commercial purposes.

DOI: 10.1002/adom.202101712

materials are prepared via the conventional drying of the hybrid nanocrystals. However, assembling the nanoscopic building blocks into macroscopic, porous, 3D gel-like structures could significantly broaden their applicability.^[18] In nanocrystal gels, the nanoscopic characteristics of the nanoparticle building blocks can be retained and novel properties can emerge simultaneously, which underlines the advantages of these assembled structures over their colloidal solutions.^[19] Upon partial removal of the stabilizing ligands from the nanocrystal surface under controlled conditions, the assembly of the nanoparticles can be initiated leading to an interconnected nanocrystal network.^[20,21] Although gel-like structures have been prepared from various materials to date, we have recently presented novel routes towards the formation of hybrid nanocrystal networks for spectroelectrochemical applications, where the preparation route (i.e., via simple mixing of different building blocks or preparing the hybrid semiconductor-noble metal nanoparticles prior to their assembly) has been found to be of central importance.^[22–26] While simple mixing and co-gelation has not led to efficient charge carrier separation, growth of the metal domains directly on the nanorods or nanoplatelets enabled to fabricate hybrid gel structures with enhanced photoelectrochemical performance. This sheds light on the impact of proper nanostructuring on the emerging properties at the macroscale.

Consequently, in the present work, our objective is to synthesize and assemble different gold decorated CdSe/CdS NRs and form macroscopic porous gel-like structures with effective charge carrier separation (schematically shown in **Figure 1**) in order to investigate the impact of particle design on the spectroelectrochemical properties of the gel networks (at the macroscale). To deposit gold domains in controlled and arbitrary manner, different synthetic approaches were applied to prepare gold tipped and randomly decorated CdSe/CdS NRs (referred to as tipped-NR and random-NR, respectively). These NRs were employed as building blocks to fabricate different semiconductor-metal hybrid aero- and xerogels to investigate the macrostructural properties upon different nanoscale design. The key difference between these gels is the significantly diverse spatial distance between the neighboring gold domains in the hybrid nanostructures. The characterization with electron microscopy, UV–vis spectroscopy and electrochemical measurements like intensity modulated photocurrent spectroscopy (IMPS) give insights into the nanoscopic structure and its influence on the

optical and spectroelectrochemical properties of the assembled networks. Here, both an oxidative method using H_2O_2 and a nonoxidative method using Y^{3+} cations were applied to destabilize the aqueous nanoparticle solutions and trigger their assembly.^[20,21]

2. Results and Discussion

2.1. Characterization of the Nanoparticle Building Blocks

The spatial control over the growth of gold domains on CdSe/CdS NRs can be achieved by adjusting the reaction parameters. This can lead to differently designed hybrid NRs: the selective growth on the tips of the NRs as well as the growth of gold on defect sites along the NRs.^[5,27] In this work, a slightly modified method following Menagen et al. has been applied to synthesize the above-mentioned gold tipped-NR and the random-NRs.^[5] This offers two nanostructuring routes: (i) the light-induced growth procedure leads to the selective growth of gold on the preferred sulfur rich facets which are located at the tip of the NR, with the size of the domains being controlled by the reaction time. Gold is reduced directly by the photoexcited electrons supporting the growth on the preferred facets forming tipped NRs. (ii) Using a thermal growth mechanism (namely without irradiation during the growth process), reduction of gold is induced on several defect sites along the semiconductor NRs via the amine being present in the solution. This manifests itself in a form of randomly decorated hybrid nanoparticles. The morphology and optical properties of the hybrid particles using the selective growth mechanisms are demonstrated in **Figure 2**, where the transmission electron microscopy (TEM) images and the extinction spectra are shown before and after the phase transfer from organic to aqueous solutions. In the extinction spectra, the spectroscopic features of the semiconductor as well as of the metal can be observed. The rise in the extinction at 600 nm is correlated to the CdSe core and at 450 nm to the CdS rod. Tipped-NR and random-NR systems show additionally the localized surface plasmon resonance (LSPR) of the gold with a maximum between 500 and 600 nm. Differences between the tipped-NR and random-NR systems in the wavelength range of 480–700 nm can be attributed to the difference in the size of the grown gold domains. The domains on the randomly decorated

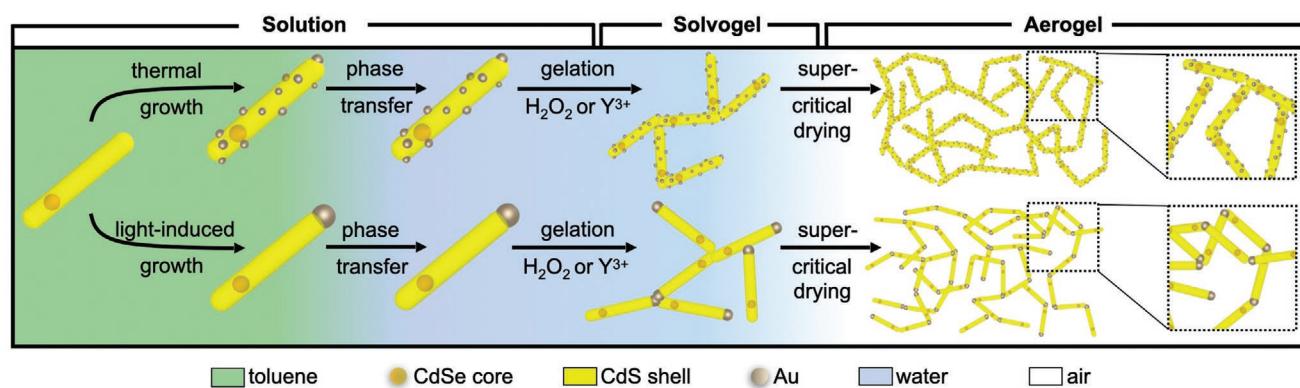


Figure 1. Schematic pathways from CdSe/CdS NRs to gold decorated gel networks using two different approaches.

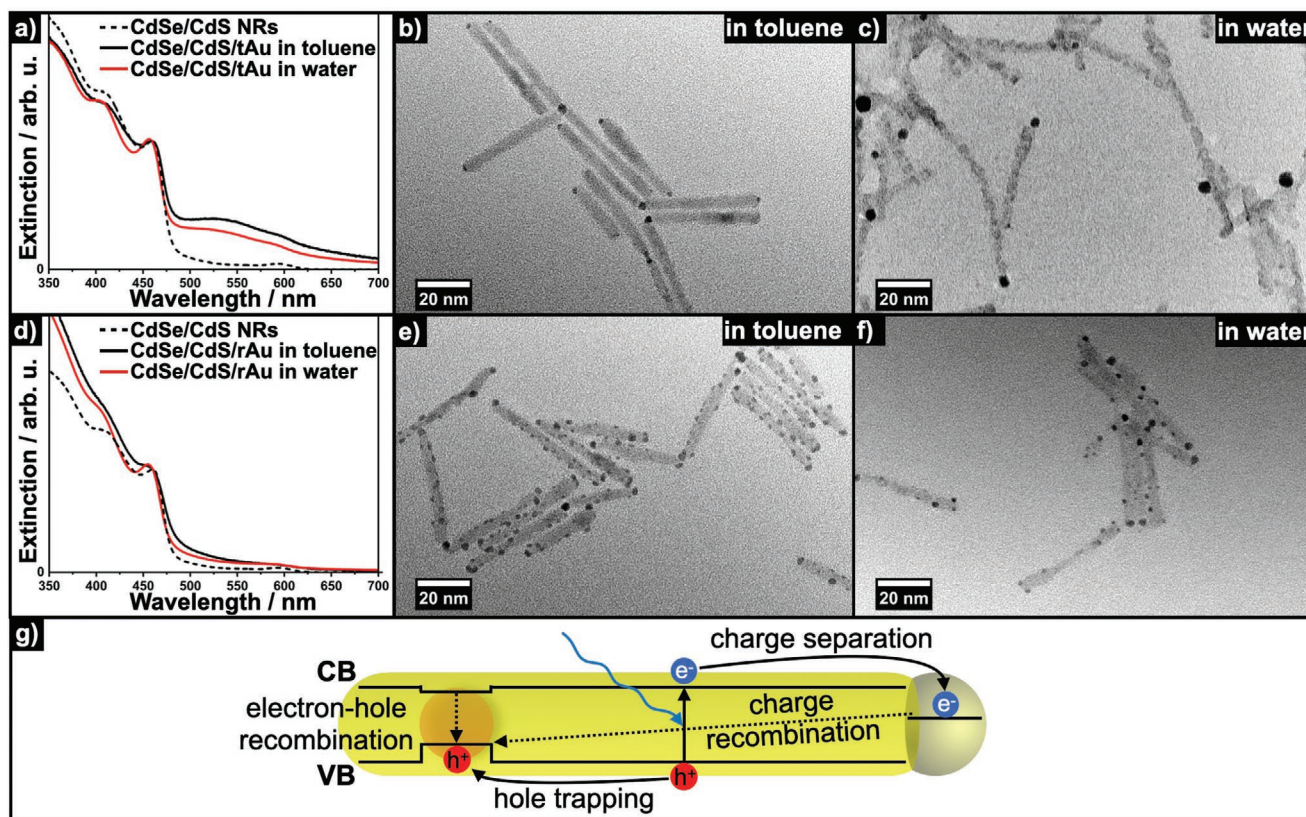


Figure 2. Extinction spectra in toluene and water (solid lines) compared to the spectrum of pure CdSe/CdS NRs in toluene (dashed line) and TEM images of a–c) tipped-NRs and d–f) random-NRs. g) Scheme of the electronic band structure of a gold decorated CdSe/CdS NR with the governing charge carrier processes upon illumination.

NRs are slightly smaller (2.0 ± 0.5 nm) compared to the gold tips (3.0 ± 1.4 nm), that alters their contribution to the extinction spectra due to different scattering and absorption cross sections of smaller and larger gold domains.^[28]

A phase transfer of the hybrid particles to aqueous solutions is required to trigger the assembly of the nanoparticle solution using H_2O_2 (to partially oxidize the surface ligands) or Y^{3+} cations (to partially remove and cross-link the ligands).^[20,21,29] By exchanging the TOP/TOPO ligands with the water soluble mercaptopropionic acid (MPA), the gold decorated particles were transferred to an aqueous solution by retaining the morphology of the gold decoration achieved in organic medium (Figure 2). To ensure the deprotonation of the carboxyl groups of MPA, alkaline pH is generally used during the phase transfer, that can be reached by the addition of tetramethylammonium hydroxide (TMAOH) or potassium hydroxide (KOH).^[30] In case of our hybrid particle systems, however, highly basic conditions led to the dissolution and detachment of the gold domains (Figure S3, Supporting Information). Therefore, the phase transfer was carried out without addition of extra base, hence the morphology of the gold decoration could be retained as shown in the comparative TEM images of Figure 2.

The electronic band structure of the synthesized semiconductor-metal hybrid NRs is shown in Figure 2c. Due to the quasi-type II band structure of the CdSe/CdS NR and the Fermi level of the gold which lies in between the valence- and the

conduction band of the semiconductors, spatial separation of the excited charge carriers can be achieved.^[14] Electrons delocalized along the CdS shell are transferred to the metal domains within the picosecond range while holes become located in the CdSe core.^[14] The fast electron transfer to the metal domains and a long lifetime of the electrons in the gold (up to microseconds) enable the accumulation of electrons in the metal domain leading to a rise of the Fermi level upon irradiation.^[31] This efficient charge carrier separation and the electron accumulation accomplish promising properties for catalytic applications such as hydrogen evolution reaction (HER). Building up a connected network from the hybrid nanoparticles opens up new routes towards the utilization of the above-mentioned charge carrier separation. The delocalization of the electrons upon illumination can be observed throughout connected CdSe/CdS NRs which can enable the enhanced electron transfer to the metal domains.^[20,21]

2.2. Structural Characterization of the Semiconductor-Metal Nanoparticle Gel Networks

The formation of a macroscopic network structure from the differently designed hybrid NRs has been achieved by destabilizing the nanoparticle solutions with two different methods. Using H_2O_2 as destabilizing agent leads to the oxidation of the surface-attached MPA followed by a slow assembly of the

NRs into a network of connected particles.^[32] H_2O_2 at slightly elevated temperatures ($80^\circ C$) oxidizes the thiolated ligands (RS^-) to a radical (RS^\bullet) opening available active sites for the assembly.^[29] The slow oxidation due to low concentrations of the H_2O_2 enables the controlled formation of the network consisting of mainly tip-to-tip, crystal-to-crystal connected NRs.

As we have shown recently, trivalent cations in contrast destabilize the nanoparticle solution in a nonoxidative way without thermal activation.^[21] Cations like Y^{3+} have a high affinity to the surface of the metal and the semiconductor and thus are able to remove the ligands from the surface. Using this method, active sites for the assembly are formed which leads to the connection of the nanorods. Eventually a nanoparticle gel network is formed in a controlled manner. Additionally, the cations interact via Coulomb forces with the anionic carboxylic groups of the MPA which as well supports the assembly of the nanoparticles. Although the TEM analysis of the connections between CdSe/CdS NRs formed with both H_2O_2 and Y^{3+} showed crystal contact between the building blocks, Y^{3+} cations resulted in a somewhat larger contact area and thus a stronger contact between the nanorods (Figure 3).^[21]

At this stage, nanostructuring meets macrostructuring: the assembly of the semiconductor-metal hybrid nanoparticles leads to 3D, porous structures with the retained morphology of the gold decorated building blocks. The oxidative as well as the nonoxidative destabilization procedures results in gold

decorated semiconductor solvogels, from which monolithic aerogels can be prepared upon drying the structures in a critical point dryer (using supercritical CO_2). Scanning electron microscopy (SEM) images show the voluminous, porous 3D structure and the macroscopic character of the gel networks whereas the TEM images give an insight of the nanoscopic morphology and the position of the gold domains in the formed interconnected NR network (Figure 3).

Arbitrary and controlled spatial deposition of noble metal domains have impact on the structural properties of the gel materials. Assembling the random-NRs, a network with gold on the sides of the nanorods and additionally in many cases as the (partial) connection between the NRs is formed. A network from the tipped-NRs results in gold only in the connection points between the NRs. Mostly, the gold domains are located in-between the NRs, however, some direct rod-to-rod connections without gold can also be observed due to the single-tipped nature of the building blocks (i.e., one tip is non-decorated). In comparison to the random-NR network, the distance between two gold domains (<10 nm in case of tipped and ≈ 40 nm for random-NRs) and the size of the domains are larger (3.2 ± 1.2 nm in case of tipped and 2.0 ± 0.6 nm for random-NRs). Due to the larger distance between them, an extended mobility (enhanced spatial delocalization) of the electrons in the tipped-NR network is expected, which was expected to alter their spectroelectrochemical properties.

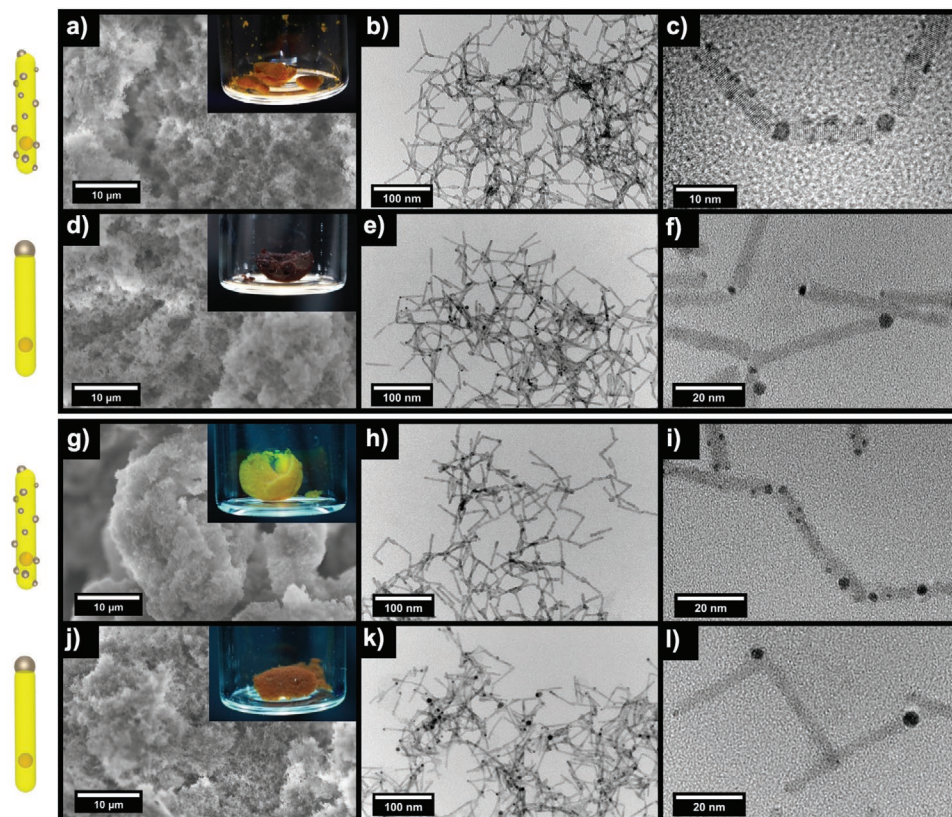


Figure 3. Comparative morphological overview of different hybrid aerogel networks assembled via a–f) H_2O_2 (upper panel) and g–l) Y^{3+} (lower panel). SEM images (a, d, g, j) and TEM images of random-NR aerogels assembled via H_2O_2 (b, c) and Y^{3+} (h, i) as well as tipped-NR aerogels assembled via H_2O_2 (e, f) and Y^{3+} (k, l). Insets of the SEM images show the photographs of the macroscopic aerogel monoliths.

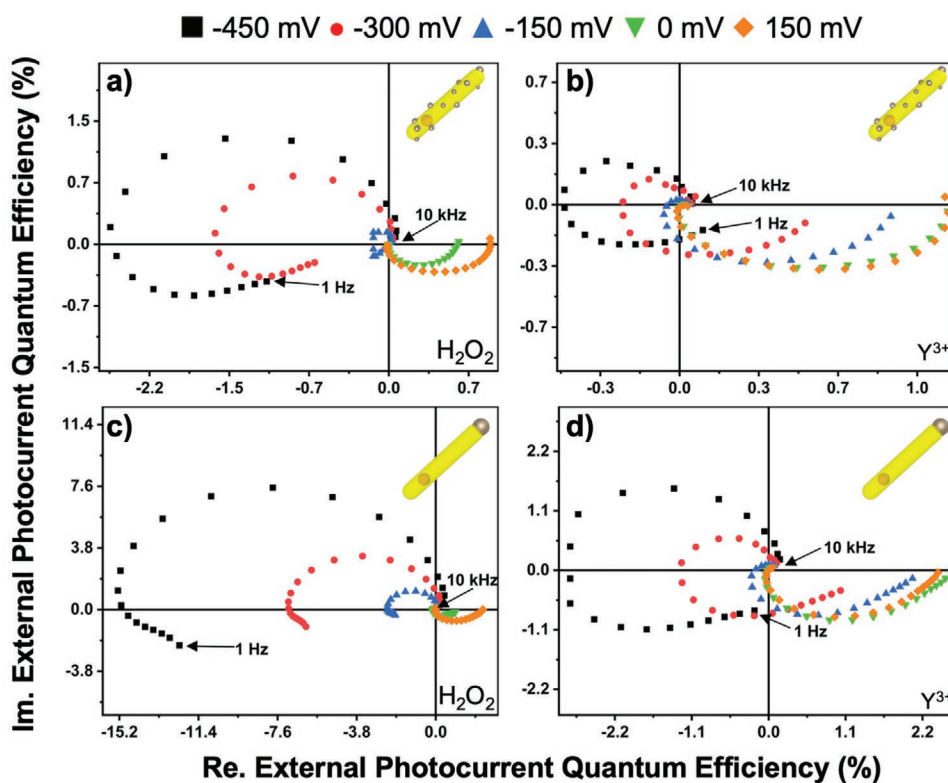


Figure 4. Nyquist plots of the IMPS response of random-NR xerogel networks formed with a) H_2O_2 and b) Y^{3+} and of tipped-NR xerogel networks formed with c) H_2O_2 and d) Y^{3+} .

2.3. Spectroelectrochemical Investigation of the Semiconductor-Metal Nanoparticle Gel Networks

To investigate the effect of the nanostructuring on the spectroelectrochemical properties (charge carrier dynamics) of the hybrid macrostructures, intensity modulated photocurrent spectroscopy (IMPS) was applied on xerogel samples (see Figure S7 in the Supporting Information for the experimental setup).^[33] IMPS is a frequency-resolved spectroscopic technique, where a frequency-modulated light source excites a photoelectrochemically active electrode which is under potentiostatic control. In the applied measurements, the working electrode consists of the nanoparticle network deposited on a conductive substrate. As a response to the frequency-modulated light (in the range of 1 Hz to 10 kHz), a photocurrent with a certain intensity and phase shift compared to the intensity and phase of the incoming light can be detected. In a Nyquist plot, the real and imaginary IMPS datapoints result in semicircles and can be interpreted with the knowledge of the charge carrier transfer processes in the investigated system. In **Figure 4**, the photoelectrochemical response of indium tin oxide (ITO) electrodes coated with the different xerogel networks (measured in an aqueous 0.5 M Na_2SO_3 solution at pH = 9 which acts as a hole scavenger) are shown. While pure ITO electrodes (without gel structures) do not show active electrochemical processes (see Figure S10 in the Supporting Information), positive and negative photocurrents can be observed in the xerogel electrodes under illumination which represent two major photoelectrochemical processes. The transfer of electrons from the

network to the electrode and the scavenging of the hole by sulfite ions from the electrolyte lead to positive photocurrent, whereas the electron transfer from the network to solution by reducing protons to hydrogen results in negative photocurrent (the main photoinduced electrochemical processes are detailed in Figure S8 in the Supporting Information). For the discussion of the results and the proposed mechanism only the course of the photocurrent and not the absolute values have been used. Although all samples have been prepared in the same way, the exact amount of the electrode material cannot be entirely unified, thus, the absolute values of the photocurrent might slightly differ. Consequently, the photocurrent response and its characteristics as a function of the bias potential and the frequency of the light pulses are used for the interpretation.

In the IMPS spectra, a different behavior of the networks upon applying positive and negative bias potentials can be observed. Positive photocurrent dominates at bias potentials of 0 and +150 mV, while negative photocurrent with a turnaround towards the positive photocurrent direction can be observed for 150, 300, and 450 mV, respectively (Figure 4). This turnaround indicates the competition between processes leading to positive and negative photocurrents. The negative photocurrent becomes more remarkable at high frequencies. In contrast, the positive photocurrent becomes more pronounced at lower frequencies. These observations are also supported by linear sweep voltammetry measurements, which show the evolution of the positive and negative photocurrents at different bias potentials in time as well (Figure S9, Supporting Information). Comparing the networks of random and tipped-NRs indicates

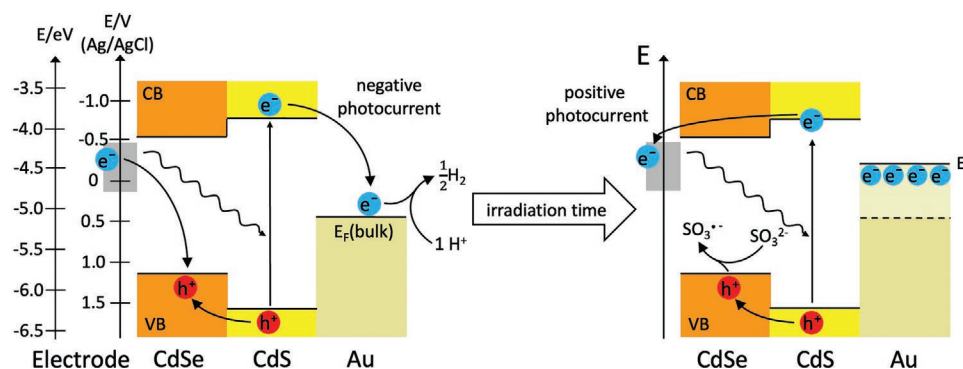


Figure 5. Schematic illustration of the energy landscape of the heteronanoparticle, the electron accumulation, and the rise of the Fermi level in the metal domain upon longer irradiation time and the subsequent change of the photocurrent direction. The conduction band offset at the CdSe/CdS heterojunction is around 0.23 eV, which leads to the formation of a quasi-type II alignment.^[15] For the positioning of the Au Fermi level, the bulk value was used (−5.1 eV), which can rise upon being contacted with a semiconductor surface^[36] but still remains within the band gap of the CdS shell.

that the tipped network reaches higher photocurrent quantum efficiencies regarding the negative as well as the positive photocurrent. Furthermore, the semicircles show an elongated shape at lower frequencies, which is less pronounced at negative bias potentials and not observed at positive bias potentials for the random-NR networks. The different destabilization methods show minor differences in the high frequency range. A less extensive turnaround at negative bias potentials in case of H₂O₂ destabilized networks and the elongation at positive bias potentials for the tipped network is slightly more pronounced in case of the Y³⁺ destabilized network.

2.4. Mechanism of the Charge Carrier Dynamics

Based on the above-discussed observations, a model for the charge carrier dynamics can be derived. **Figure 5** depicts the estimated energy landscape of the heteronanoparticles and illustrates the evolution of negative and positive photocurrents. Upon irradiation of the semiconductor-metal hybrid gel networks, the excited electrons are accumulated in the metal domains regardless of the location of the gold on the NRs. This is supported by the intrinsically small conduction band energy difference (≈ 0.23 eV) between the CdSe core and the CdS shell that makes the electron delocalization possible over the NR.^[15,19,34,35] Nevertheless, the main driving force of the electron extraction from the semiconductor into the noble metal domain is the Fermi level of the gold located in the band gap of the CdS.^[36] Electrons from the gold domains favorably reduce protons and form hydrogen, due to their longer lifetime in the metal domains and the catalytic activity of the metal. This leads to an increasing negative photocurrent with decreasing frequency of the light pulses (Figure S8, Supporting Information). In semiconductor-metal hybrid nanoparticles, not only the contact between the metal and the semiconductor,^[36] but the electron accumulation inside the Au upon irradiation might also be able to raise the Fermi level of the gold domain.^[31,37] On the one hand, with further decreasing frequency (i.e., increasing irradiation times), the Fermi level of the gold domains raises and the electron transfer from the conduction band of the semiconductor to the gold domains becomes less favorable while

the electron transfer to the electrode becomes more favorable (Figure 5). Furthermore, with the accumulation of the electrons and the holes, the possibility of charge carrier recombination increases due to the increasing Coulomb forces between the electrons and the holes. Additionally, for the random-NR network, tunneling processes between the gold domains can also occur which was shown by Lavieville et al. where shorter distances between metal domains led to an increased conductivity.^[38] The higher tunneling probability and thus shorter distances to the holes in random-NR networks leads to a larger recombination rate.^[39–41] Although in Figure 5, solely the vicinity of the electrode is depicted, these effects can also take place further from the electrode surface due to the NR–NR connections throughout the network.

The turnaround to more positive photocurrent with decreasing frequency can be explained with the raise of the Fermi level and the increasing recombination rate due to the accumulation of the electrons in the metal domains. Higher photocurrent quantum efficiencies for the tipped-NR network indicate a more efficient charge carrier separation and thus a more efficient electron transfer towards the electrolyte. Another feature which is observed for the tipped-NR network is the elongation of the semicircles at low frequencies having a positive bias potential. The elongation results when electrons from further distances reach the electrode, which is observed at lower frequencies due to the larger timescale of the electron transport through the network.^[21,42,43] Thus, the elongation suggests electron mobility within the semiconductor network, and consequently indicates larger metal-to-metal domain distances in the interconnected tipped structure. These tipped structures possess only one Au domain on each semiconductor NR which leads as well to semiconductor–semiconductor contacts that enable the electron delocalization and transport within larger parts of the network. This cannot be observed in the randomly decorated particle network, where the structural properties clearly showed remarkably smaller spatial distances (less than 10 nm) between the gold domains hindering the free electron movement across the connected NRs. Due to the better connection between the rods in case of the Y³⁺ destabilized networks, the electron seems to be more free to travel in these architectures compared to the H₂O₂ destabilized ones. That agrees well

with the findings regarding the larger contact areas between the NRs in such cases.^[21]

In comparison to the particle networks, we have shown earlier the spectroelectrochemical properties of random-NR particles as submonolayers.^[41] In case of individual particles on ITO, no turnaround to more positive photocurrents can be observed which is correlated to the connection of the particles to the ITO electrode and the missing contact between the NRs. Electrons in the gold domains can easily tunnel to the ITO electrode which hinders the accumulation of the electrons in the metal domains and thus the rise of the Fermi level. With this the photocurrent direction does not change with increasing frequency. Instead, for hybrid gel structures as investigated in the present work, the NR–NR connections have a higher impact on the charge carrier dynamics compared to submonolayers, where the contribution of the NR-ITO interface to the IMPS response is significantly overrepresented.

As it has recently been demonstrated by Banin et al., the catalytic activity of gold in hybrid nanostructures shows size dependency.^[11,44] The overall catalytic efficiency depends on the efficiency of electron transfer from the semiconductor to the metal domain and on the catalytic activity of the metal domain itself. Both show opposite dependencies regarding the size of the metal domains, and thus, an optimal metal domain size can be found to maximize the activity. Importantly, this size-effect of the gold domains in our networks cannot be simply correlated with the observed photoelectrochemical differences, since the optimal gold domain size is around 2 nm.^[11] According to this, a higher negative photocurrent for the random-NR network would be expected, which however, cannot be observed due to another important effect: the increased recombination rate in the random-NR network (due to the much smaller spatial distances between the Au domains) overweighs the auspicious gold domain size resulting in a lower observed photocurrent efficiency.

3. Conclusion

To conclude, 3D networks of interconnected CdSe/CdS/Au semiconductor–metal hybrid nanoparticles have been prepared. Different spatial distribution of the gold domains can be achieved by assembling randomly decorated and tipped CdSe/CdS/Au hybrid nanoparticles into 3D, hyperbranched networks. Using two different gelation routes for both types of building blocks, highly porous, voluminous, and branched aerogels have been obtained in all cases. In form of xerogels deposited on conductive substrates, all these gold-decorated networks show an effective charge carrier separation, which leads to the accumulation of the electrons in the metal domains upon irradiation. Intensity modulated photocurrent spectroscopy has revealed the effect of the spatial distance between the metal domains on the charge carrier separation efficiency. More efficient charge carrier separation has been found in the tipped-NR networks resulting in higher negative photocurrent efficiencies compared to the random-NR networks where the charge recombination is more pronounced. Our results imply that the design of the hybrid nanoparticles plays central role in the electrochemical properties of the assembled macrostructures, i.e.,

nanostructuring has a vast impact on the properties of macroscopic gel networks. Control over the location of metal domains on the building blocks—compared to the arbitrary decoration—facilitates a more effective charge carrier separation. Beside the nanoscale particle design, the linking procedure (gelation route) is of central importance in the tailoring of the interparticle interactions and, thus, the macrostructuring of different semiconductor-metal hybrid NPs with high application potential in photoelectrocatalysis and energy harvesting.

Supporting Information

Supporting Information is available from the Wiley Online Library or from the author.

Acknowledgements

J.S. and D.Z. contributed equally to this work. The authors would like to acknowledge the financial support of the European Research Council (ERC) under the European Union's Horizon 2020 research and innovation program (grant agreement 714429). Additionally, this work was funded by the German Research Foundation (Deutsche Forschungsgemeinschaft, DFG) under Germany's excellence strategy within the cluster of excellence PhoenixD (EXC 2122, project ID 390833453) and the grant BI 1708/4-1. A.S. is thankful for financial support from the Hannover School for Nanotechnology (hsn). Moreover, the authors thank Armin Feldhoff and Jürgen Caro for providing the SEM facility. Furthermore, the used TEM for the shown images was provided by the Laboratory of Nano and Quantum Engineering.

Open access funding enabled and organized by Projekt DEAL.

Conflict of Interest

The authors declare no conflict of interest.

Data Availability Statement

Research data are not shared.

Keywords

aerogels, charge carrier separation, hybrid-nanoparticle network, photoelectrochemistry, self-assembly

Received: August 17, 2021
Revised: September 23, 2021
Published online: October 29, 2021

- [1] Y. Hu, S. Mignani, J. P. Majoral, M. Shen, X. Shi, *Chem. Soc. Rev.* **2018**, *47*, 1874.
- [2] I. Balti, A. Barrère, V. Gueguen, L. Poussard, G. Pavon-Djavid, A. Meddahi-Pellé, P. Rabu, L. S. Smiri, N. Jouini, F. Chaubet, *J. Nanopart. Res.* **2012**, *14*, 1266.
- [3] S. Kundu, A. Patra, *Chemical Reviews* **2017**, *117*, 712.
- [4] R. Costi, A. E. Saunders, U. Banin, *Angew. Chem., Int. Ed.* **2010**, *49*, 4878.

- [5] G. Menagen, J. E. Macdonald, Y. Shemesh, I. Popov, U. Banin, *J. Am. Chem. Soc.* **2009**, *131*, 17406.
- [6] A. Freytag, C. Günnemann, S. Naskar, S. Hamid, F. Lübke, D. Bahnemann, N. C. Bigall, *ACS Appl. Nano Mater* **2018**, *1*, 6123.
- [7] S. Naskar, A. Freytag, J. Deutsch, N. Wendt, P. Behrens, A. Köckritz, N. C. Bigall, *Chem. Mater.* **2017**, *29*, 9208.
- [8] P. Kalisman, L. Houben, E. Aronovitch, Y. Kauffmann, M. Bar-Sadan, L. Amirav, *J. Mater. Chem. A* **2015**, *3*, 19679.
- [9] R. Costi, A. E. Saunders, E. Elmalem, A. Salant, U. Banin, *Nano Lett.* **2008**, *8*, 637.
- [10] P. V. Kamat, *J. Phys. Chem. C* **2008**, *112*, 18737.
- [11] Y. Ben-Shahar, F. Scotognella, I. Kriegel, L. Moretti, G. Cerullo, E. Rabani, U. Banin, *Nat. Commun.* **2016**, *7*, 10413.
- [12] Y. Ben-Shahar, J. P. Philbin, F. Scotognella, L. Ganzer, G. Cerullo, E. Rabani, U. Banin, *Nano Lett.* **2018**, *18*, 5211.
- [13] N. Waiskopf, Y. Ben-Shahar, M. Galchenko, I. Carmel, G. Moshitzky, H. Soreq, U. Banin, *Nano Lett.* **2016**, *16*, 4266.
- [14] M. Waechtler, P. Kalisman, L. Amirav, *J. Phys. Chem. C* **2016**, *120*, 9.
- [15] H. Eshet, M. Grünwald, E. Rabani, *Nano Lett.* **2013**, *13*, 5880.
- [16] U. Banin, Y. Ben-Shahar, *Nat. Energy* **2018**, *3*, 824.
- [17] M. Rosebrock, D. Zámbo, P. Rusch, D. Pluta, F. Steinbach, P. Bessel, A. Schlosser, A. Feldhoff, K. D. J. Hindricks, P. Behrens, D. Dorfs, N. C. Bigall, *Adv. Funct. Mater.* **2021**, 2101628, <http://doi.org/10.1002/adfm.202101628>.
- [18] C. Ziegler, A. Wolf, W. Liu, A. K. Herrmann, N. Gaponik, A. Eychmüller, *Angew. Chem., Int. Ed.* **2017**, *56*, 13200.
- [19] P. Rusch, B. Schremmer, C. Strelow, A. Mews, D. Dorfs, N. C. Bigall, *J. Phys. Chem. Lett.* **2019**, *10*, 7804.
- [20] S. Sánchez-Paradinas, D. Dorfs, S. Friebe, A. Freytag, A. Wolf, N. C. Bigall, *Adv. Mater.* **2015**, *27*, 6152.
- [21] D. Zámbo, A. Schlosser, P. Rusch, F. Lübke, J. Koch, H. Pfnür, N. C. Bigall, *Small* **2020**, *16*, 1906934.
- [22] D. Zámbo, A. Schlosser, R. T. Graf, P. Rusch, P. A. Kißling, A. Feldhoff, N. C. Bigall, *Adv. Opt. Mater.* **2021**, *9*, 2100291.
- [23] T. Kodanek, A. Freytag, A. Schlosser, S. Naskar, T. Härtling, D. Dorfs, N. C. Bigall, *Z. für Phys. Chem.* **2018**, *232*, 1675.
- [24] S. Naskar, J. F. Miethe, S. Sánchez-Paradinas, N. Schmidt, K. Kanthasamy, P. Behrens, H. Pfnür, N. C. Bigall, *Chem. Mater.* **2016**, *28*, 2089.
- [25] W. Liu, A. K. Herrmann, N. C. Bigall, P. Rodriguez, D. Wen, M. Oezaslan, T. J. Schmidt, N. Gaponik, A. Eychmüller, *Acc. Chem. Res.* **2015**, *48*, 154.
- [26] A. Schlosser, J. Schlenkrich, D. Zámbo, M. Rosebrock, R. T. Graf, N. C. Bigall **2021**.
- [27] Y. Khalavka, S. Harms, A. Henkel, M. Strozyk, R. Ahijado-Guzmán, C. Sönnichsen, *Langmuir* **2018**, *34*, 187.
- [28] V. R. Stull, G. N. Plass, *J. Opt. Soc. Am.* **1960**, *50*, 121.
- [29] J. L. Mohanan, I. U. Arachchige, S. L. Brock, *Science* **2005**, *307*, 397.
- [30] T. Kodanek, H. M. Banbela, S. Naskar, P. Adel, N. C. Bigall, D. Dorfs, *Nanoscale* **2015**, *7*, 19300.
- [31] V. Subramanian, E. E. Wolf, P. V. Kamat, *J. Am. Chem. Soc.* **2004**, *126*, 4943.
- [32] I. U. Arachchige, S. L. Brock, *Acc. Chem. Res.* **2007**, *40*, 801.
- [33] E. A. Ponomarev, L. M. Peter, *J. Electroanal. Chem.* **1995**, *396*, 219.
- [34] G. Rainò, T. Stöferle, I. Moreels, R. Gomes, J. S. Kamal, Z. Hens, R. F. Mahrt, *ACS Nano* **2011**, *5*, 4031.
- [35] E. R. Smith, J. M. Luther, J. C. Johnson, *Nano Lett.* **2011**, *11*, 4923.
- [36] Y. Zhang, O. Pluchery, L. Caillard, A.-F. Lamic-Humblot, S. Casale, Y. J. Chabal, M. Salmeron, *Nano Lett.* **2014**, *15*, 51.
- [37] M. Jakob, H. Levanon, P. V. Kamat, *Nano Lett.* **2003**, *3*, 353.
- [38] R. Lavieville, Y. Zhang, A. Casu, A. Genovese, L. Manna, E. Di Fabrizio, R. Krahn, *ACS Nano* **2012**, *6*, 2940.
- [39] T. Simon, M. T. Carlson, J. K. Stolarczyk, J. Feldmann, *ACS Energy Lett.* **2016**, *1*, 1137.
- [40] W. Choi, J. Y. Choi, H. Song, *APL Mater.* **2019**, *7*, 100702.
- [41] J. F. Miethe, F. Lübke, J. Poppe, F. Steinbach, D. Dorfs, N. C. Bigall, *ChemElectroChem* **2018**, *5*, 175.
- [42] A. Schlosser, L. C. Meyer, F. Lübke, J. F. Miethe, N. C. Bigall, *Phys. Chem. Chem. Phys.* **2019**, *21*, 9002.
- [43] J. F. Miethe, F. Lübke, A. Schlosser, D. Dorfs, N. C. Bigall, *Langmuir* **2020**, *36*, 4757.
- [44] Y. Nakibli, Y. Mazal, Y. Dubi, M. Wächtler, L. Amirav, *Nano Lett.* **2018**, *18*, 357.